Mixed-Valence Compounds

Large Lattice Responses in a Mixed-Valence Prussian Blue Analogue Owing to Electronic and Spin Transitions Induced by X-ray Irradiation**

Serena Margadonna, Kosmas Prassides, and Andrew N. Fitch*

Mixed-valence metal cyanides with general formula $A_xM^{II}{}_y[M'^{III}(CN)_6]\cdot n\,H_2O$ (where A is an alkali-metal cation, and M and M′ are divalent and trivalent transition-metal cations, respectively) have attracted considerable interest because of their unusual electronic and magnetic properties.[1] In addition to molecular-based ferromagnetic properties with Curie temperatures higher than room temperature,[2–4] the availability of degenerate or quasidegenerate electronic states has made them ideal systems with which to explore switching phenomena at the molecular level.[5] For example, in some of these materials visible-light irradiation at low temperatures can drive optically controlled phase transitions to long-lived metastable states where the optical and/or magnetic properties change dramatically, thereby raising the potential of applications in memory devices and magneto-optical switching.[6–10] Metal-to-metal electron transfer was also induced by X-ray irradiation at very low temperatures in the Prussian blue analogue, $Rb_{1.8}Co_4[Fe(CN)_6]_{3.3}\cdot 13\,H_2O$ with the resulting phase transformation monitored by energy-dispersive synchrotron X-ray diffraction.[11] Herein, we show that X-ray irradiation can also induce interconversion between the ground and excited states in another such compound **1**, over a broad temperature range (between room temperature and 10 K). Depending on the experimental conditions, a variety of internal charge-transfer processes and spin transitions are triggered resulting in either continuous or abrupt phase transformations that are accompanied by large lattice relaxations and can be accurately monitored by high-resolution angle-dispersive synchrotron X-ray diffraction.

$Rb_{0.7}Mn^{II}{}_{1.15}[Fe^{III}(CN)_6]\cdot 2\,H_2O$ **1**

Important information concerning the thermo- and photoinduced magnetization/demagnetization behavior of transition-metal cyanides has been recently obtained by studying the cubic $RbMn^{II}[Fe^{III}(CN)_6]$ system.[12] At room temperature, the Mn^{II} ions are in their high-spin (HS, $t_{2g}{}^3e_g{}^2$, $S=5/2$) state and the Fe^{III} ions in the low-spin (LS, $t_{2g}{}^5e_g{}^0$, $S=1/2$) state, and these ions couple antiferromagnetically. Cooling induces a charge transfer from manganese to iron leading to Mn^{III} in the HS ($t_{2g}{}^3e_g{}^1$, $S=2$) and Fe^{II} in the LS state ($t_{2g}{}^6e_g{}^0$, $S=0$) and is accompanied by a cubic–tetragonal phase transition, driven by the Jahn–Teller distortion of the $Mn^{III}N_6$ octahedra[13,14] and the appearance of ferromagnetism at approximately 10 K.[15] Green light irradiation at low temperatures induces the reverse electron transfer and the low lying Mn^{II}–Fe^{III} excited state can then be populated.[16] Herein, we report on the internal redox reactions triggered by synchrotron X-ray radiation as a function of temperature and time in the related mixed-valence metal cyanide, **1**. As excited metastable electronic and spin states are populated and evolve with illumination time at different temperatures, the angle-dispersive synchrotron X-ray diffraction technique allows simultaneous complete crystal structure refinements, which leads to the elucidation of the resulting rich phase diagram in unprecedented detail.

We examined the synchrotron X-ray diffraction profiles of **1** collected at 295 K and at 100 and 10 K after cooling in the absence of X-ray illumination. No reflections violating face-centered cubic (*fcc*) extinction rules are evident and the crystal structure remains strictly cubic down to 10 K. Rietveld analysis (Figure 1a, see Supporting Information) proceeded smoothly with the generic structural model of mixed-valence metal cyanides,[17] comprising a three-dimensional network of $\{Mn(NC)_6\}$ and $\{Fe(CN)_6\}$ octahedra linked by the CN ligands (space group $Fm\bar{3}m$, $a=10.54314(4)$ Å at 295 K). The $Fe(CN)_6$ vacancy positions (13%) are occupied by H_2O molecules completing the coordination sphere of neighboring Mn^{II} cations while the Rb^+ ions are disordered in the tetrahedral interstices of the framework structure (inset Figure 1a). The Mn–N and Fe–C bond lengths of the $\{Mn(NC)_6\}$ and $\{Fe(CN)_6\}$ octahedra refine to 2.249(4) and 1.900(5) Å, respectively, consistent with the Mn^{II}-NC-Fe^{III} ground state (GS) assignment of the metal valence states. This result is also in agreement with the magnetic susceptibility data (measured $\chi T=5.17\ cm^3\,K\,mol^{-1}$ at 295 K; spin-only value calculated for Mn^{II}(HS, $S=5/2$)-Fe^{III}(LS, $S=1/2$), $\chi T=5.41\ cm^3\,K\,mol^{-1}$). In contrast to stoichiometric

[*] Dr. S. Margadonna
Department of Chemistry
University of Cambridge
Cambridge CB2 1EW (UK)
Fax: (+44) 1223-336-362
E-mail: sm413@cam.ac.uk
Prof. K. Prassides
Department of Chemistry
University of Sussex, Brighton BN1 9QJ (UK)
Dr. A. N. Fitch
European Synchrotron Radiation Facility
38042 Grenoble (France)

[**] We thank the ESRF for synchrotron X-ray beamtime, the Royal Society for a Dorothy Hodgkin Research Fellowship (S.M.), and Dr. M. Kurmoo (Strasbourg) for useful discussions.

Supporting information for this article is available on the WWW under http://www.angewandte.org or from the author.

  DOI: 10.1002/ange.200460603

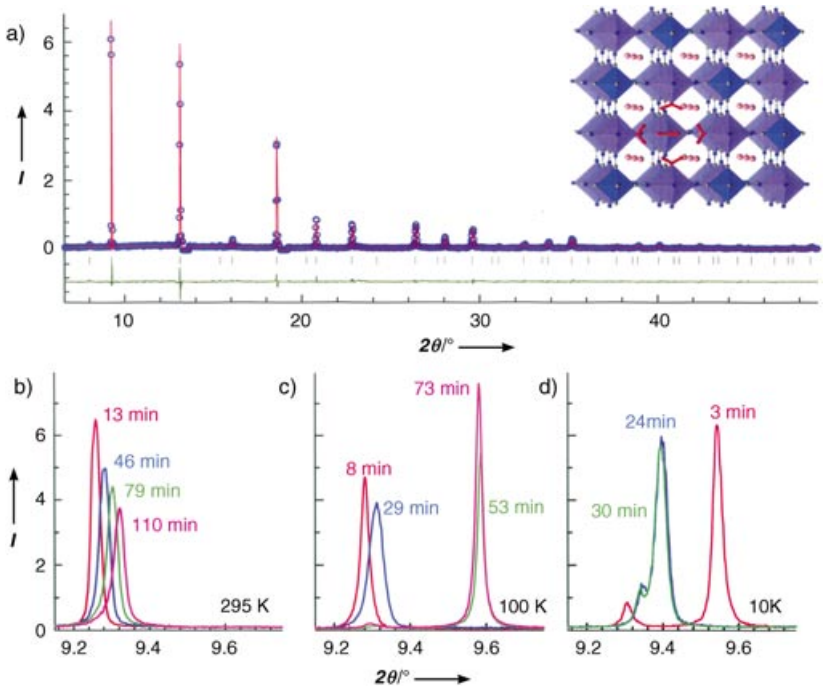

Figure 1. a) Final observed (blue circles) and calculated (red solid line) synchrotron X-ray powder diffraction profiles ($\lambda = 0.85066$ Å) for **1** at 295 K after 17 min of X-ray illumination. The lower green solid line shows the difference profile and the tick marks show the reflection positions. Two impurity peaks were excluded from the refinement. Inset: Building block of the cubic framework structure of **1**. Alternating $\{Mn(NC)_6\}$ (light violet) and $\{Fe(CN)_6\}$ (dark violet) octahedra are bridged by CN ligands. Pink spheres Rb^+ ions, red H_2O molecules residing in the $Fe(CN)_6$ vacancies. b)–d) Selected region of representative diffraction profiles showing the evolution of the (200) Bragg reflection with increasing X-ray illumination time. b) 295 K, c) 100 K, d) 10 K. Each curve is labeled with the corresponding illumination time.

$RbMn[Fe(CN)_6]$, which is tetragonal at low temperatures[13,14] after an internal electron transfer to give ferromagnetically coupled Mn^{III}(HS, $S=2$)–Fe^{II}(LS, $S=0$)–Mn^{III}(HS, $S=2$) units, no phase change is observed for **1** down to 10 K. This result can be understood in terms of the disorder associated with the water molecules which fill the $Fe(CN)_6$ vacancies, thereby suppressing the cubic–tetragonal phase transition of stoichiometric $RbMn[Fe(CN)_6]$ and is consistent with the temperature dependence of the magnetic data (see Supporting Information), which show 1) a change in χT below 180 K to 4.5 $cm^3 K mol^{-1}$, implying that the thermally induced charge transfer to give Mn^{III}(HS, $S=2$)–Fe^{II}(LS, $S=0$) occurs only partially (<20%) on cooling, 2) a negative Weiss temperature of −5.4 K implying predominant Mn^{II}–Fe^{III} antiferromagnetic interactions at low temperatures, and 3) the appearance of weak ferrimagnetism below approximately 10 K (coercive field = 235 Oe, remnant magnetization = 240 $cm^3 G mol^{-1}$).

We monitored the evolution of the diffraction profiles at various temperatures with increasing exposure time to the X-ray radiation. A striking feature of the data at 295 K is that, although the structure remains cubic, the diffraction peaks continuously shift to higher angles (Figure 1b), which implies that the material rapidly contracts at a rate of 0.238(3) $Å^3 min^{-1}$ (Figure 2a) and shows an overall volume decrease after 150 min of 2.9%. It is remarkable that the lattice contraction at 295 K for the illuminated sample is large enough to produce a cell volume considerably smaller than that of the non-illuminated sample at 10 K (overall volume decrease ca. 0.5%). Rietveld refinements with the same $Fm\bar{3}m$ structural model reveal a monotonic decrease of the Mn–N bond length to 2.203(4) Å after 150 min of exposure of the sample to the X-ray beam (Figure 2b) at room temperature. This result is consistent with a progressive generation of Mn^{III}-NC-Fe^{II} centers with increased X-ray illumination time and shrinking of the Mn–N bonds upon oxidation of the Mn^{II} centers. In contrast, the iron coordination sphere changes very little upon reduction as expected (in $K_3[Fe(CN)_6]$ Fe^{III}–C 1.93 Å, and in $K_4[Fe(CN)_6]$ Fe^{II}–C 1.91 Å[8]). Though there is no unique real-space description of this internal charge-transfer effect, the observation that the width of the diffraction peaks also progressively increases (see Figure 1b) leads us to describe the observed X-ray induced transformation as the formation of Mn^{III}-NC-Fe^{II} islands which progressively grow in size within a matrix of the original Mn^{II}-NC-Fe^{III} units and with a local structure different from that of the average bulk structure.

The behavior of **1** is even more intriguing when the X-ray irradiation is switched on at 100 K after cooling without illumination (Figure 1c). The diffraction peaks initially shift continuously to higher angles as at 295 K but, after an incubation period of approximately 20 min, all the diffraction peaks are accompanied by a partner at significantly higher angle, thereby providing the signature of a sudden transformation of the high-temperature structure to an isostructural one (PT-1) with drastically reduced lattice dimensions (Figure 2a). The fraction of the contracted phase grows rapidly in a very short time and is accompanied by a notable sharpening of the diffraction peaks, which indicates the occurrence of a phase transition in the bulk. The abrupt collapse in the unit cell dimensions ($\Delta V/V \approx -10.3\%$) can be again understood in terms of the X-ray induced internal redox process Mn^{II}(HS)-NC-Fe^{III}(LS)→Mn^{III}(HS)-NC-Fe^{II}(LS), which occurs even more efficiently at this temperature. This process leads to a large fraction of photoconverted units that exceeds the percolation threshold and thereby a cooperative first-order phase transformation is abruptly triggered. Rietveld refinements (see Supporting Information) indicate that in the contracted phase, the Mn–N bond length further shortens significantly to 2.056(5) Å, while the Fe–C bond lengthens only slightly to 1.920(5) Å (Figure 2b). We note that the abrupt phototransformation to the collapsed phase is accompanied by the appearance of a small fraction (ca. 5%) of a coexisting minority phase whose lattice

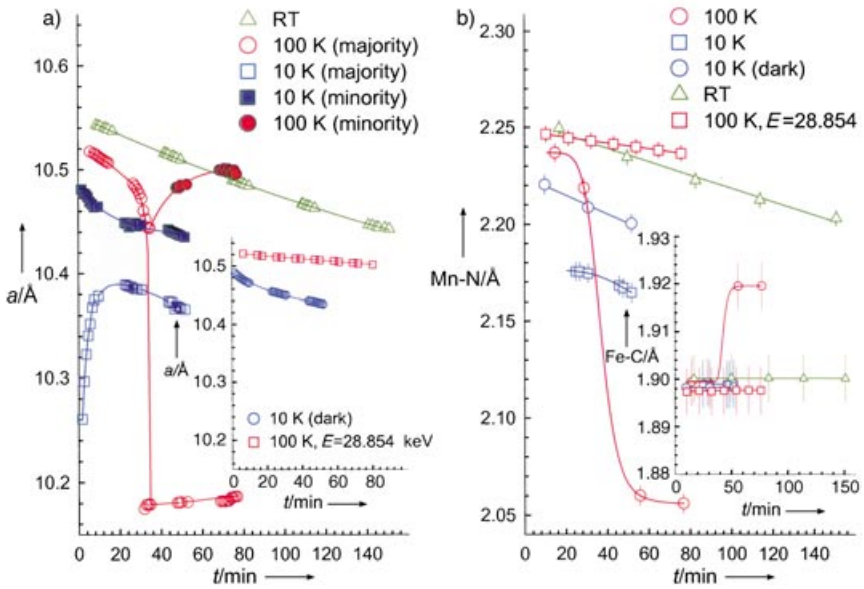

Figure 2. a) Evolution with increasing X-ray ($E = 14.575$ keV) illumination time of the cubic lattice constant in **1** at different temperatures: 295 K (green triangles), 100 K (red circles), 10 K (blue squares). Open symbols represent the lattice constants of the majority (full symbols the minority) phases at 100 and 10 K. Inset: the time dependence of the lattice constants at 10 K ($E = 14.575$ keV) after cooling in the dark (blue circles) and at 100 K for an incident photon energy of 28.854 keV (red squares). b) The corresponding time evolution of the Mn–N (inset: Fe–C) bond lengths as obtained from Rietveld refinements of the synchrotron X-ray powder diffraction profiles. Symbols are as described in (a).

size rapidly increases and approaches that expected for the untransformed material at this temperature (Figure 2a). Complementary experiments at 100 K with an X-ray beam of energy 28.854 keV were not able to induce the same first-order transition even after 80 min of irradiation and led only to a very slow decrease of the lattice dimensions at a rate of 0.083(2) $Å^3 min^{-1}$ (inset Figure 2a). This can be understood by the now significantly reduced (by a factor between about 40–80) energy per unit volume per second deposited at the sample rendering the phototransformation extremely inefficient. This conclusion is also supported by the extracted lattice constant ($a = 10.49667(4)$ Å) being similar to that of the untransformed minority phase at 14.575 keV ($a = 10.4877(7)$ Å). In a complementary series of diffraction experiments at 100 K with a synchrotron X-ray beam of energy 28.850 keV, the first-order transformation to the collapsed phase was also successfully triggered by continuous wave (CW) green laser light illumination ($\lambda = 532$ nm, power = 50 mW).[18]

Substantial changes to the diffraction profile of the phototransformed PT-1 material are also observed on cooling to 10 K (Figure 1d). An extremely rapid phase change sets in as soon as the X-ray light is switched on and the lattice size inflates within the first 10 min by $\Delta V/V \approx +6.3\,\%$. Apparently the PT-1 phase, which was accessed at 100 K by X-ray irradiation now becomes highly unstable and transforms to a new bulk phase (PT-2) whose lattice constants straddle those of PT-1 and of the non-irradiated phase (GS; see Supporting Information). Undoubtedly, the formation of PT-2 is triggered by the reverse internal redox process, which led to the formation of PT-1 from GS, namely Mn^{III}-NC-$Fe^{II} \rightarrow Mn^{II}$-NC-$Fe^{III}$. However, both the reduced lattice dimension ($a = 10.36940(6)$ Å) and refined Mn–N bond distance of 2.168(5) Å (Figure 2) are inconsistent with a description of the electronic states of the bridging motifs as identical to those of GS, namely Mn^{II}(HS)-NC-Fe^{III}(LS). Additional support for the conclusion that the phototransformed PT-2 phase should not be identified with GS comes from the presence of a co-existing minority phase (9.9(1)%) with a lattice size identical to that of the material when cooled to 10 K in the dark (Figure 2a) and therefore comprising Mn^{II}(HS)-NC-Fe^{III}(LS) units.

To our knowledge, such a sensitivity to X-ray light with facile interconversion between a number of metastable states with differing charge (electronic) and spin (magnetic) states through both continuous (second order) and discontinuous (first order) phase transitions at temperatures ranging from 10 K to room temperature has not been reported for a single molecular system. It is reminiscent of the transitions from an insulating antiferromagnetic to a metallic ferromagnetic state in the $Pr_{0.7}Ca_{0.3}MnO_3$ manganite[19,20] and from a charge-ordered spin-dimerized to a disordered dimer state in the $CuIr_2S_4$ spinel[21] that were driven by X-ray illumination at low temperatures (< 40 K and < 10 K, respectively). Stabilization of the photoinduced states in the manganites has been strongly linked to the structural changes, which accompany the absorption of X-ray photons and the relaxation of the lattice distortion associated with the $\{Mn^{III}O_6\}$ octahedra. This is a similar mechanism to that developed herein for the mixed-valence metal cyanides in which the photoinduced long-range-ordered states at 100 and 10 K are stabilized by the large lattice relaxations after electron removal from the $\{Mn^{II}(NC)_6\}$ octahedra or electron addition to $\{Mn^{III}(NC)_6\}$ octahedra. Moreover, our picture of the inhomogeneous character of the continuous phototransformation at room temperature is also analogous to that proposed for both the manganites and the spinels,[19–21] in which the X-ray induced states are similarly characterized by structural inhomogeneities, as evidenced by the observed peak broadening and gradual evolution in the unit cell dimensions and metal–ligand bond lengths.

In conclusion, the initial results presented herein open the way for the study of the structural relaxations of otherwise inaccessible metastable electronic states of various multistable molecular materials following the absorption of photons. In addition, given the energy tunability of synchrotron X-ray light, the kinetics of the phototransformations can be controlled and moved between different time windows even at ambient temperature. We also note the considerably persistent character of the photoinduced transitions. To explain this, we can invoke the large lattice relaxations, which in these materials accompany the internal charge transfer and spin rearrangements (strong electron–phonon

coupling) and need large energies in order to be annealed. Figure 3 summarizes the postulated electronic and spin configurations of the transition-metal ions following the X-ray-driven first-order phase transition at 100 K. Although the optical and magnetic properties of the two photoinduced bulk states, PT-1 and PT-2 are not probed in the present diffraction experiments directly, we anticipate that both their color and their magnetization should also significantly change. For instance, the color of the material exposed to X-ray light at room temperature changes from light to dark brown. Comparing the magnetic properties, we note that the untransformed material comprises antiferromagnetically coupled Mn^{II}(HS, $S = 5/2$) and Fe^{III}(LS, $S = 1/2$) ions and becomes ferrimagnetic at about 10 K. On the other hand, the exchange coupling between near-neighbor Mn^{III}(HS, $S = 2$) ions in PT-1 is mediated by the Fe^{III}(LS, $S = 0$) degenerate t_{2g} orbitals and is of ferromagnetic nature. As a result, conversion into the phototransformed excited states should be accompanied by drastic changes of the magnetization.

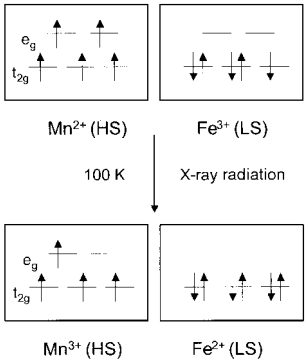

Figure 3. Schematic representation of the postulated electronic and spin configurations of the Mn and Fe ions following the X-ray-induced first-order phase transitions at 100 K in **1** at an incident photon energy of 14.575 keV.

Experimental Section

1 was prepared as a light brown solid by reaction of aqueous solutions of $MnCl_2$ (0.1M), RbCl (1M), and $K_3Fe(CN)_6$ (0.1M) and its stoichiometry established by elemental (Rb:Mn:Fe = 0.72:1.13:1) and thermogravimetric analysis. Temperature- and field-dependent magnetization measurements were performed with a Quantum Design MPMS5 SQUID susceptometer. For the angle-dispersive synchrotron X-ray diffraction measurements, samples were sealed in thin-wall glass capillaries 0.5 mm in diameter. With the sample inside a continuous-flow cryostat, synchrotron X-ray powder diffraction data ($\lambda = 0.85066$ Å, $E = 14.575$ keV, beamsize approximately 2.3×1.4 mm^2) were collected on cooling at 295, 100, and 10 K as a function of illumination time using the high-resolution powder X-ray diffraction beamline ID31 at the European Synchrotron Radiation Facility (ESRF), Grenoble, France. Complementary diffraction data were also collected at 100 K using X-rays with $\lambda = 0.42970$ Å ($E = 28.854$ keV). Data analysis was performed with the GSAS suite of Rietveld analysis programs.

Received: May 9, 2004
Revised: August 2, 2004

Keywords: electron transfer · mixed-valence compounds · phase transitions · photochemistry · Prussian blue analogues · solid-state structures

[1] P. Gütlich, Y. Garcia, T. Woike, *Coord. Chem. Rev.* **2001**, *219*, 839.
[2] S. Ferlay, T. Mallah, R. Ouahes, P. Veillet, M. Verdaguer, *Nature* **1995**, *378*, 701.
[3] Ø. Hatlevik, W. E. Buschmann, J. Zhang, J. L. Manson, J. S. Miller, *Adv. Mater.* **1999**, *11*, 914.
[4] S. M. Holmes, G. S. Girolami, *J. Am. Chem. Soc.* **1999**, *121*, 5593.
[5] S. Ohkoshi, K. Hashimoto, *J. Photochem. Photobiol. C* **2001**, *2*, 71.
[6] O. Sato, T. Iyoda, A. Fujishima, K. Hashimoto, *Science* **1996**, *272*, 704.
[7] O. Sato, Y. Einaga, A. Fujishima, K. Hashimoto, *Inorg. Chem.* **1999**, *38*, 4405.
[8] A. Bleuzen, C. Lomenech, V. Escax, F. Villain, F. Varret, C. Cartier dit Moulin, M. Verdaguer, *J. Am. Chem. Soc.* **2000**, *122*, 6648.
[9] H. W. Liu, K. Matsuda, Z. Z. Gu, K. Takahashi, A. L. Cui, R. Nakajima, A. Fujishima, O. Sato, *Phys. Rev. Lett.* **2003**, *90*, 167403.
[10] M. Hanawa, Y. Moritomo, A. Kuriki, J. Tateishi, K. Kato, M. Takata, M. Sakata, *J. Phys. Soc. Jpn.* **2003**, *72*, 987.
[11] V. Escax, A. Bleuzen, J. P. Itie, P. Munsch, F. Varret, M. Verdaguer, *J. Phys. Chem. B* **2003**, *107*, 4763.
[12] S. Ohkoshi, H. Tokoro, M. Utsunomiya, M. Mizuno, M. Abe, K. Hashimoto, *J. Phys. Chem. B* **2002**, *106*, 2423.
[13] Y. Moritomo, K. Kato, A. Kuriki, M. Takata, M. Sakata, H. Tokoro, S. Ohkoshi, K. Hashimoto, *J. Phys. Soc. Jpn.* **2002**, *71*, 2078.
[14] K. Kato, Y. Moritomo, M. Takata, M. Sakata, M. Umekawa, N. Hamada, S. Ohkoshi, H. Tokoro, K. Hashimoto, *Phys. Rev. Lett.* **2003**, *91*, 255502.
[15] Y. Moritomo, A. Kuriki, K. Ohoyama, H. Tokoro, S. Ohkoshi, K. Hashimoto, N. Hamada, *J. Phys. Soc. Jpn.* **2003**, *72*, 456.
[16] Y. Moritomo, M. Hanawa, Y. Ohishi, K. Kato, M. Takata, A. Kuriki, E. Nishibori, M. Sakata, S. Ohkoshi, H. Tokoro, K. Hashimoto, *Phys. Rev. B* **2003**, *68*, 144106.
[17] H. J. Buser, D. Schwarzenbach, W. Petter, A. Lüdi, *Inorg. Chem.* **1977**, *16*, 2704.
[18] The observed photoinduced effects are of persistent nature. Upon switching off the X-ray beam and warming the sample in the dark to room temperature, the lattice contraction partially survives for many hours (after 10 h, the fraction of the collapsed phase is still about 20%), which implies that the lattice strains accompanying electron transfer are large enough that relaxation does not occur immediately even at room temperature. However, we note that if in the course of warming to room temperature the sample is continuously illuminated by green laser light, the pristine room temperature phase (GS) is completely recovered.
[19] V. Kiryukhin, D. Casa, J. P. Hill, B. Keimer, A. Vigliante, Y. Tomioka, Y. Tokura, *Nature* **1997**, *386*, 813.
[20] D. E. Cox, P. G. Radaelli, M. Marezio, S.-W. Cheong, *Phys. Rev. B* **1998**, *57*, 3305.
[21] H. T. Ishibashi, Y. Koo, Y. S. Hor, A. Borissov, P. G. Radaelli, Y. Horibe, S.-W. Cheong, V. Kiryukhin, *Phys. Rev. B* **2002**, *66*, 144424.

